

Analysis of NACA 2412 Airfoil in ANSYS Fluent (ASME V&V 20-2009)

Abstract

This project focuses on the aerodynamic analysis of the NACA 2412 airfoil, utilizing computational fluid dynamics (CFD) techniques to study its performance under varying conditions. The airfoil was designed in ANSYS Design Modeler, and a C-shaped computational domain was created to simulate airflow around the airfoil. A structured mesh was generated with particular attention to the boundary layer resolution, ensuring a Y^+ value of 1 or less to accurately capture the boundary layer effects.

The simulation was set up in ANSYS Fluent, where the lift coefficient (C_l) and drag coefficient (C_d) were analyzed and compared against experimental data for validation. Additionally, velocity and pressure contours were generated to visualize the flow behavior around the airfoil. To further investigate the airfoil's performance, the angle of attack was varied, and its impact on aerodynamic factors, including lift and drag, was studied. Y^+ was plotted to ensure proper boundary layer effects were observed.

The results provide insights into the flow characteristics, boundary layer effects, and aerodynamic efficiency of the NACA 2412 airfoil. Graphs and images from the analysis highlight key trends and validate the airfoil's performance in subsonic flow conditions. This study contributes to understanding the aerodynamic behavior of cambered airfoils and their suitability for various engineering applications.

Introduction

Airfoils play a critical role in determining the aerodynamic performance of aircraft, turbines, and various engineering applications. Among the widely studied airfoil profiles, the NACA 2412 has gained significant attention due to its balanced characteristics of lift, drag, and predictable stall behavior. Designed by the National Advisory Committee for Aeronautics (NACA), the NACA 2412 features a maximum camber of 2% at 40% of the chord length and a maximum thickness of 12%, making it suitable for subsonic flow conditions.

This project focuses on analyzing the aerodynamic behavior of the NACA 2412 airfoil at a Reynolds number of 3.1×10^6 , which is representative of real-world operational conditions. The analysis was performed using computational fluid dynamics (CFD) tools to simulate airflow around the airfoil and study key parameters such as lift coefficient (C_l), drag coefficient (C_d), and flow characteristics. A particular emphasis was placed on capturing the effects of the boundary layer by ensuring a Y^+ value of 1 or less, providing high accuracy in near-wall flow simulations.

The airfoil was designed in ANSYS Design Modeler, and a C-shaped computational domain was created to mimic real-world airflow conditions. A structured mesh was generated, with careful attention to the boundary layer resolution to capture subtle effects such as separation and transition. Simulations were conducted in ANSYS Fluent, where the lift and drag coefficients were validated against experimental data, and flow characteristics were visualized through velocity and pressure contours. Additionally, the angle of attack was varied to study its impact on aerodynamic performance and determine the airfoil's efficiency under different flight conditions.

This study provides a comprehensive analysis of the NACA 2412 airfoil, contributing to a deeper understanding of its aerodynamic behavior and suitability for applications where efficiency and stability

are critical. The findings, supported by detailed graphs and visualizations, validate the simulation results and offer insights into the practical implications of cambered airfoils in engineering design.

Methodology

Theoretical Background

Airfoil performance is fundamentally governed by key aerodynamic principles, including the Bernoulli equation, boundary layer theory, and flow separation mechanics.

1. Bernoulli Principle: The relationship between pressure and velocity in a fluid explains how pressure differentials create lift. Over the NACA 2412, higher velocities on the upper surface result in a low-pressure region, whereas the lower surface experiences a higher pressure zone, leading to lift.
2. Boundary Layer Theory: The boundary layer, a thin region of fluid adjacent to the airfoil surface, significantly influences drag and lift. By resolving the boundary layer accurately using Y^+ values below 1, viscous effects and flow separation phenomena can be reliably captured.
3. Adverse Pressure Gradient (APG): A critical concept in aerodynamics, APG occurs when pressure increases in the flow direction, often near the trailing edge of airfoils. This gradient can lead to boundary layer separation if the flow lacks sufficient energy.

Creating Airfoil Curve File

The airfoil geometry for NACA 2412 was generated using a NACA 4-digit airfoil generator. The X and Y coordinates were exported into an Excel sheet, where the Z-coordinate was removed since the geometry is 2D. To ensure the trailing edge was closed, adjustments were made to the dataset by assigning the final points as 0 and deleting other redundant coordinates. The file was saved as a .CSV file and imported into ANSYS Design Modeler (Fig. 1).

Creating Geometry: Airfoil Import and C-Type Domain

1. The .CSV file was imported into Design Modeler, and a curve was generated to define the airfoil geometry (Fig. 2).
2. The “Surface from Edges” operation was applied to create a body by selecting the airfoil edges (Fig. 3).
3. A C-shaped domain was sketched around the airfoil using an arc (radius = 7.5 m) and horizontal/vertical lines to close the domain (Fig. 4-5).
4. Two vertical lines were added near the leading and trailing edges to ensure a fine and structured mesh (Fig. 6).
5. The sketches were converted to line bodies using the “Line from Sketch” operation. The outer edges of the domain were selected to generate the body (Fig. 7).
6. Using the Boolean operation, the airfoil body was subtracted from the domain to designate the airfoil as a solid and the domain as fluid (Fig. 8).

Meshing

1. The “Suppress Line Body” operation was applied before meshing.
2. Three mesh sizing types were applied (Fig 9) :
 - o Green arrows: Mesh sizing 1.
 - o Red arrows: Mesh sizing 2.
 - o Blue arrows: Mesh sizing 3.
3. A fine structured mesh with 250 divisions was generated for accurate boundary layer resolution (Fig. 10).
4. To ensure $Y+ < 1$, the first cell height was calculated as 0.00822905 mm (Fig. 11-15).

Simulation Setup

1. Solver Selection: Pressure-based, steady time (Fig. 16).
2. Viscous Model: k- ω (2-equation).
3. Material Properties: Air viscosity set to 1.802e-05.
4. Boundary Conditions:
 - o Inlet velocity: X = 45.6 m/s, Y = 0 m/s (Fig. 17).
 - o Outlet gauge pressure: 0.
5. Reference Values: Taken from inlet conditions (Fig. 18).
6. Solution Criteria:
 - o Residuals set to 1e-06 (Fig. 19).
 - o Drag/Lift coefficients defined (Fig. 20).

Results and Discussion

Zero Degree Angle of Attack

1. Lift Coefficient (Cl): 0.21.
2. Drag Coefficient (Cd): 0.0092.
3. Comparison with experimental data (Cl = 0.25, Cd = 0.0065):
 - o Lift accuracy: 84%, error: 16%.
 - o Drag accuracy: 70%, error: 30% (Fig. 22).
4. Velocity Contours:
 - o Stagnation point and boundary layer effects observed (Fig. 23-26).

5. Pressure Contours:
 - Upper surface: Low pressure.
 - Lower surface: High pressure (Fig. 27).

Adverse Pressure Gradient Analysis

At the trailing edge, flow encounters an adverse pressure gradient (APG), leading to separation and turbulence. This phenomenon reduces lift and increases drag. Fig. 27 illustrates the gradient's impact on boundary layer separation and efficiency loss. Strategies to mitigate APG include:

- Optimizing airfoil camber.
- Reducing trailing-edge thickness.

8 Degree Angle of Attack

1. Velocity Components:
 - $X = 45.156 \text{ m/s}$, $Y = 6.346 \text{ m/s}$ (Fig. 28-30).
2. Lift Coefficient (C_l): 1.0491.
3. Drag Coefficient (C_d): 0.014167.
4. Comparison with experimental data (Fig. 32-34)
($C_l = 1.05$, $C_d = 0.0115$)
 - Lift accuracy: ~100%.
 - Drag accuracy: Significant discrepancy.
5. Contours:
 - Increased lift and drag due to higher pressure differential (Fig. 34-36).
6. Stall Prediction:
 - Increased angle of attack leads to flow separation and loss of lift beyond stall angle.

Verification of Y+ (Boundary Layer Resolution)

This verification step aligns with ASME V&V 20-2009 standards, ensuring that the boundary layer resolution is validated with proper computational fluid dynamics (CFD) practices. The adherence to these standards enhances the credibility and reliability of the simulation results. The verification of $Y+$ (Fig. 37) further strengthened the accuracy of the boundary layer modeling, ensuring the resolution was sufficient to capture viscous effects.

Uncertainty Analysis

A comprehensive uncertainty analysis was performed to assess the reliability of the computational results for lift and drag coefficients. The total uncertainty was calculated by combining systematic error (bias), random error (precision), and measurement uncertainty using the root-sum-square (RSS) method (Fig 38).

Key Terms:

Systematic Error (Bias): The deviation between the computational results and the experimental data.

Random Error (Precision): The variability in results due to solver settings, mesh resolution, or numerical methods.

Measurement Uncertainty: Error associated with the experimental setup or measurement tools.

Results:

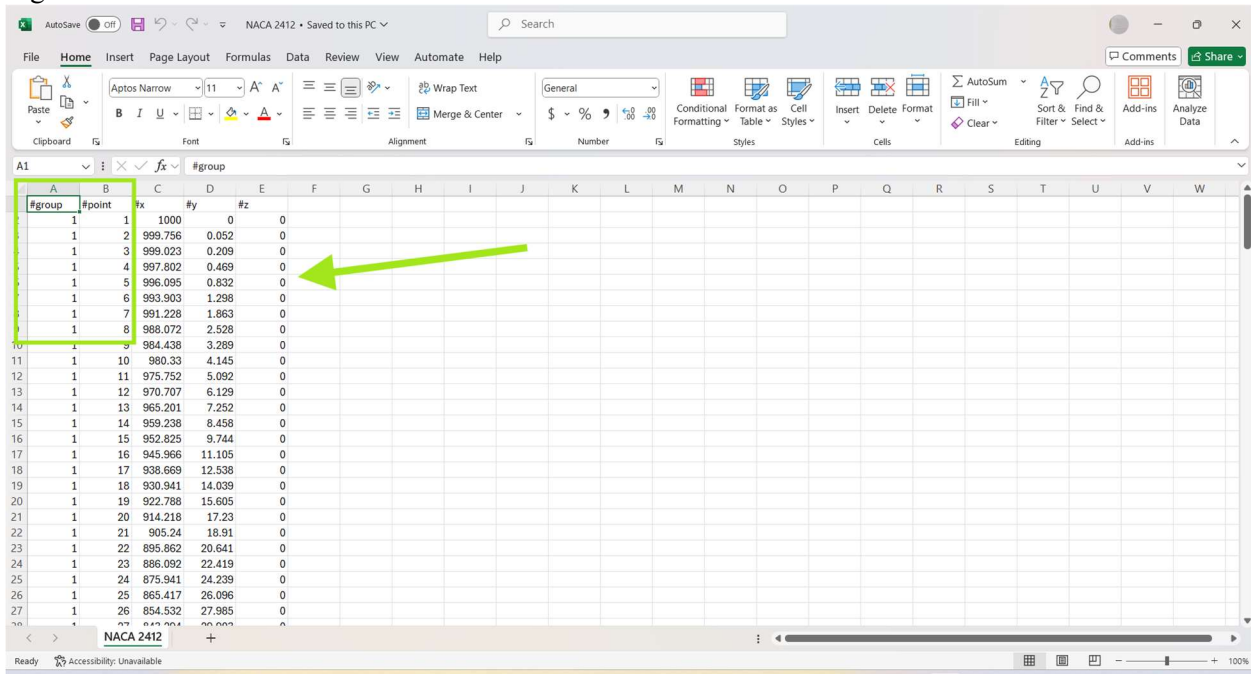
1. **Lift Coefficient (Cl):**
2. At 0° Angle of Attack: Total uncertainty = 0.040361.
3. At 8° Angle of Attack: Total uncertainty = 0.005297.
4. **Drag Coefficient (Cd):**
5. At 0° Angle of Attack: Total uncertainty = 0.002762.
6. At 8° Angle of Attack: Total uncertainty = 0.002721.
7. These values indicate that the lift predictions are highly reliable, particularly at higher angles of attack, while drag predictions show slightly higher sensitivity to measurement and simulation conditions

Conclusion

The study demonstrated the aerodynamic performance of the NACA 2412 airfoil using CFD simulations in ANSYS Fluent. The results validate the lift characteristics with experimental data, highlighting the significance of proper boundary layer resolution for accurate drag predictions. A full uncertainty analysis confirmed the reliability of the computational results, especially for lift coefficients, while also identifying areas for improvement in drag predictions. Future work can involve 3D effects and compressibility for higher Reynolds numbers.

Appendix

Fig 1



A screenshot of a Microsoft Excel spreadsheet titled "NACA 2412". The data is organized into columns A through W. Column A contains the row number, column B contains the point index, and columns C through E contain the coordinates (#x, #y, #z). A green arrow points to the coordinate values for point #2, which are 999.756 and 0.052. The table has a header row and 27 data rows. The formula bar at the top shows "#group". The status bar at the bottom indicates "Ready" and "Accessibility: Unavailable".

#group	#point	#x	#y	#z
1	1	1000	0	0
1	2	999.756	0.052	0
1	3	999.023	0.209	0
1	4	997.802	0.469	0
1	5	996.095	0.832	0
1	6	993.903	1.298	0
1	7	991.228	1.863	0
1	8	988.072	2.528	0
10	9	984.438	3.289	0
11	10	980.33	4.145	0
12	11	975.752	5.092	0
13	12	970.707	6.129	0
14	13	965.201	7.252	0
15	14	959.238	8.458	0
16	15	952.825	9.744	0
17	16	945.966	11.105	0
18	17	938.669	12.538	0
19	18	930.941	14.039	0
20	19	922.788	15.605	0
21	20	914.218	17.23	0
22	21	905.24	18.91	0
23	22	895.862	20.641	0
24	23	886.092	22.419	0
25	24	875.941	24.239	0
26	25	865.417	26.096	0
27	26	854.532	27.985	0
28	27	843.204	29.002	0

Fig 2

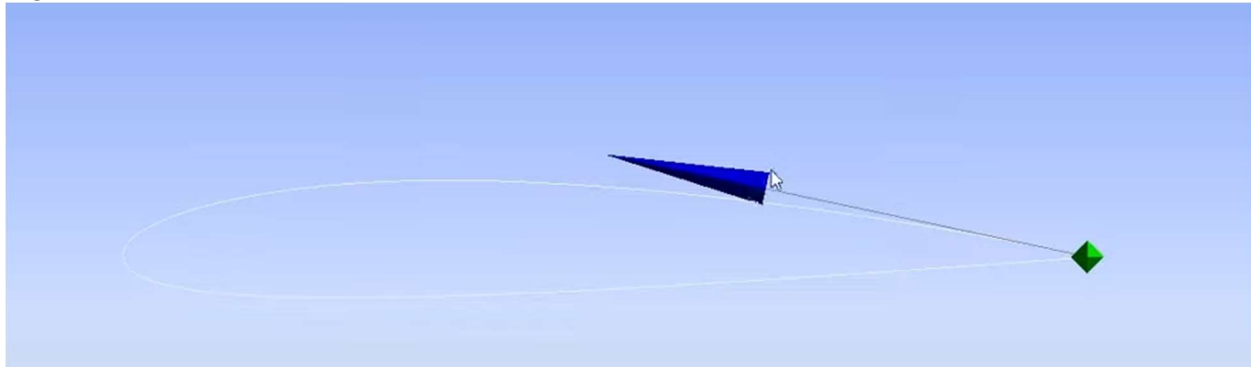


Fig 3

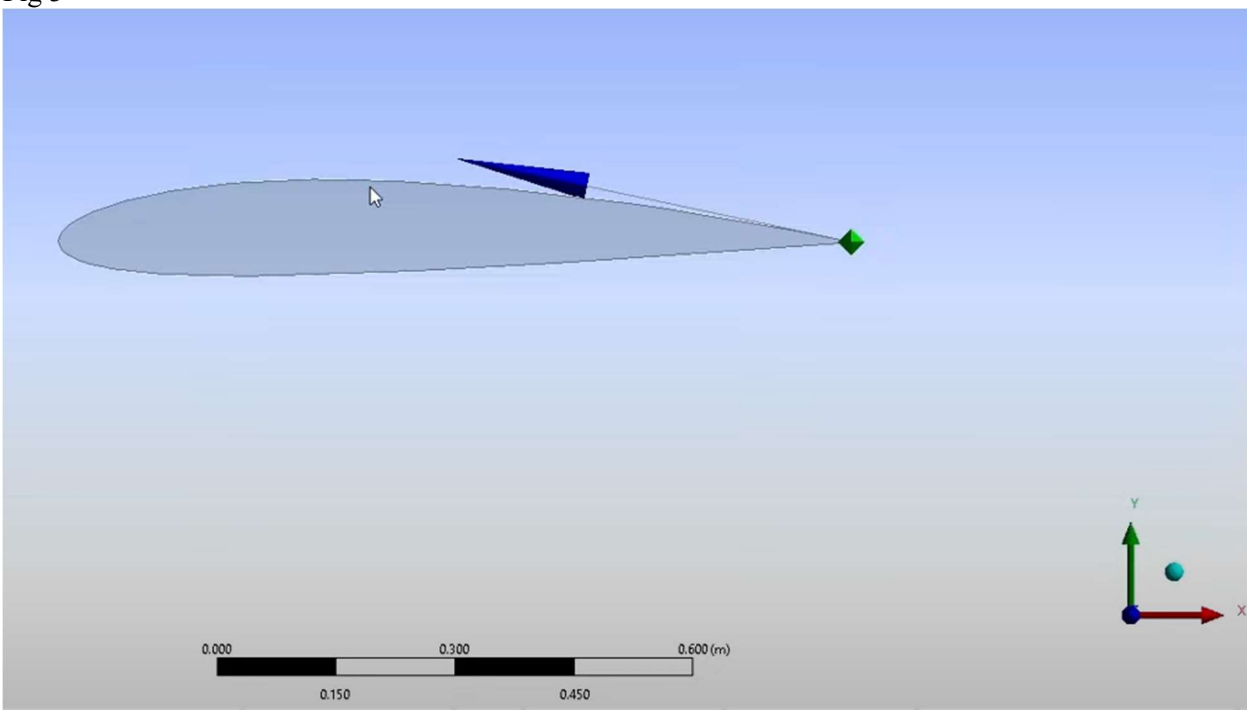


Fig 4

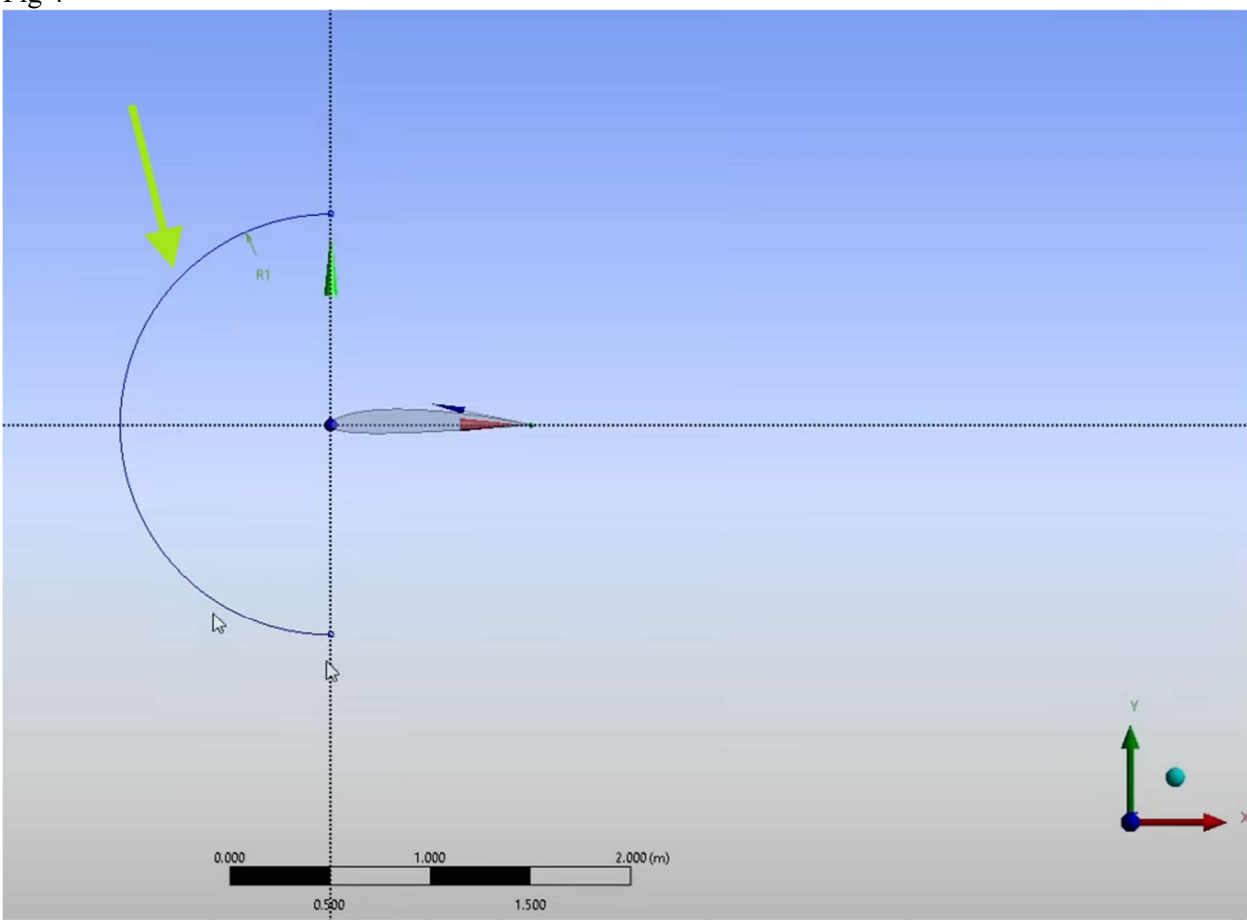


Fig 5

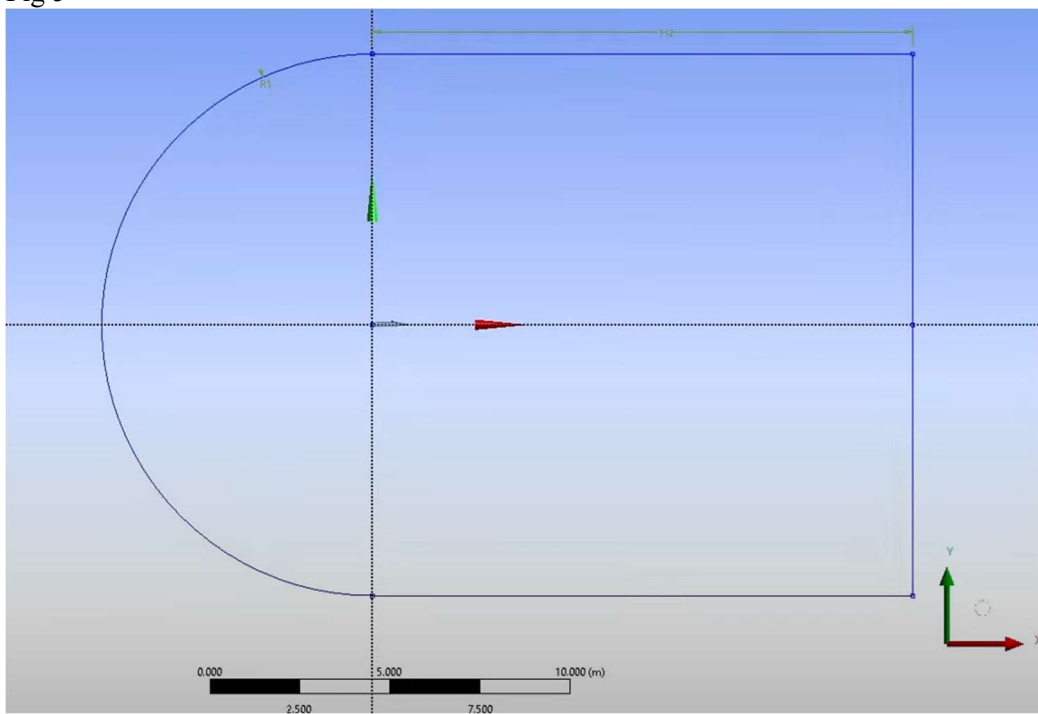


Fig 6

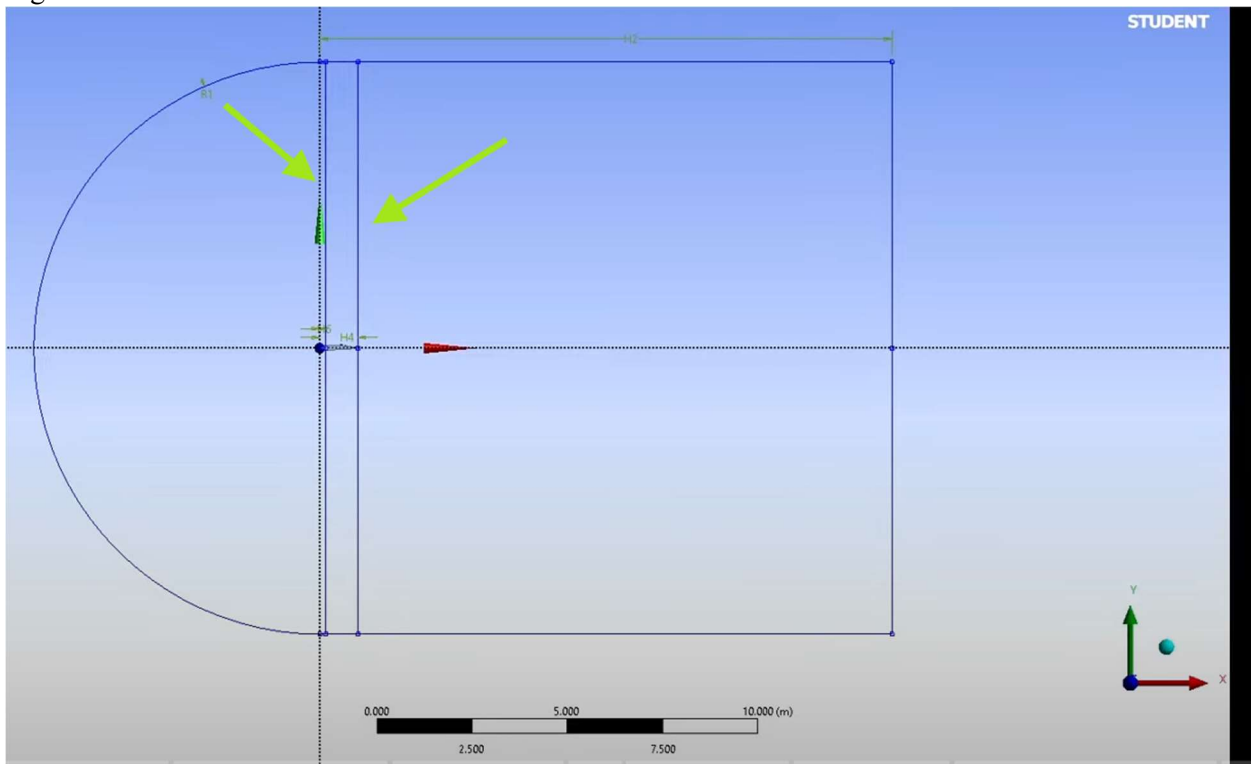


Fig 7

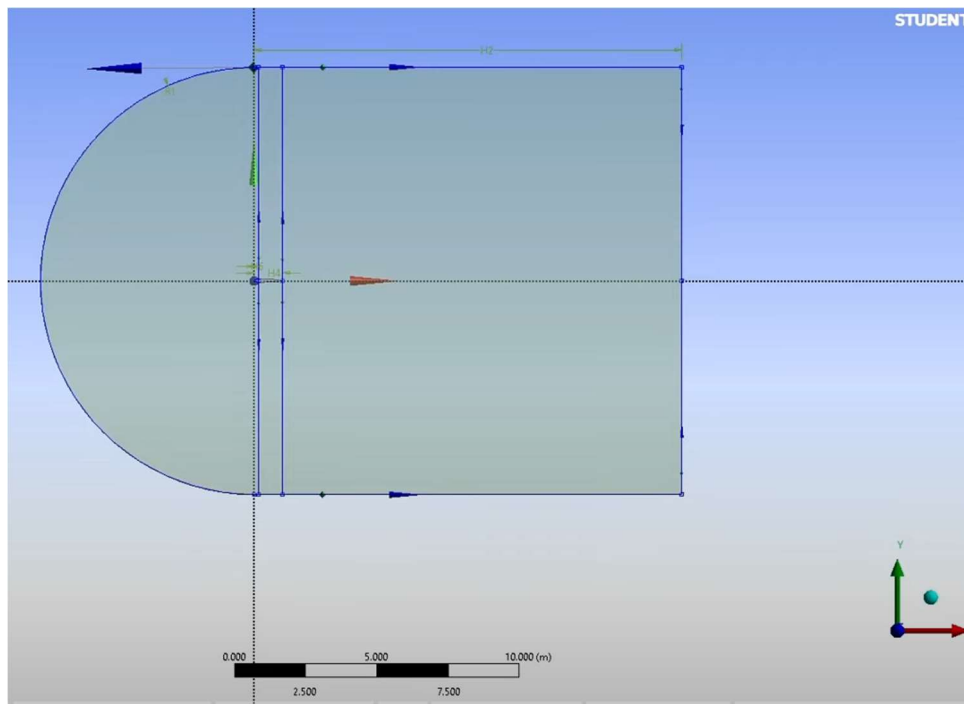


Fig 8

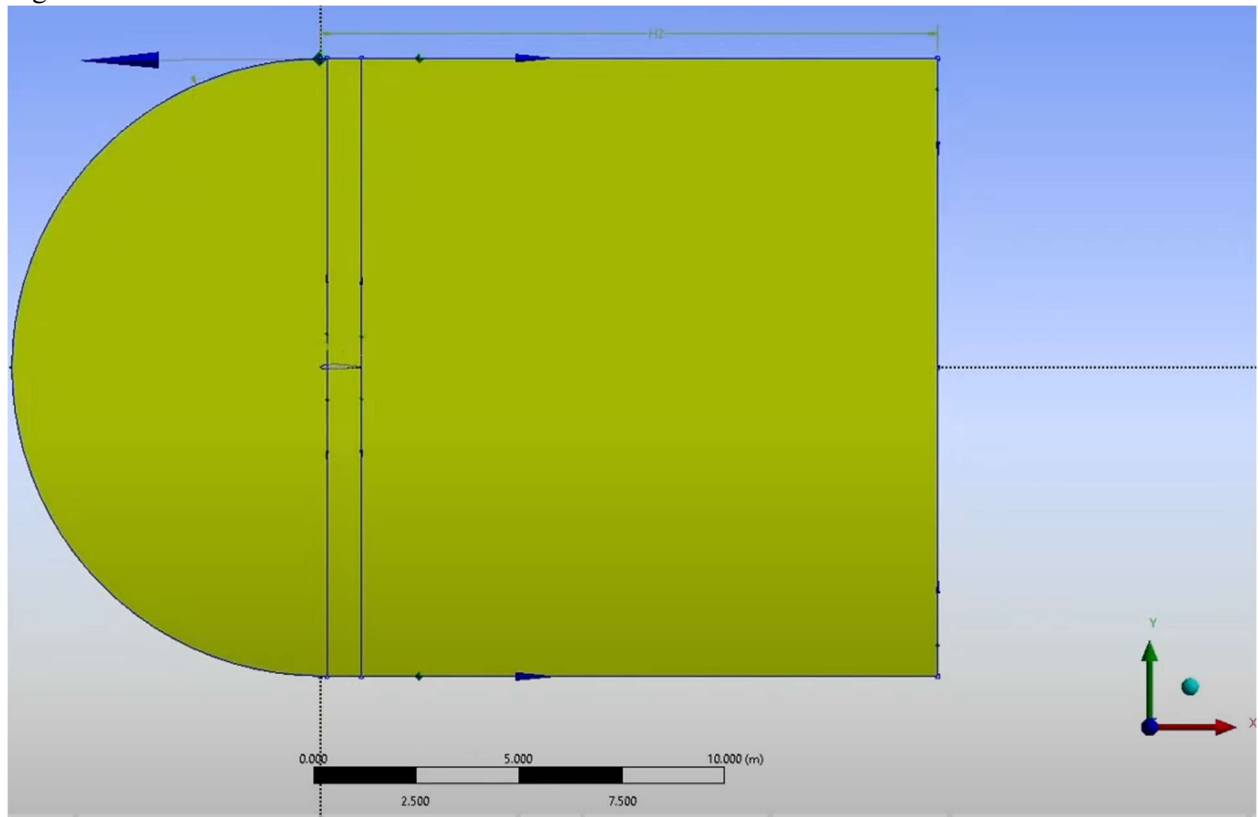


Fig 9

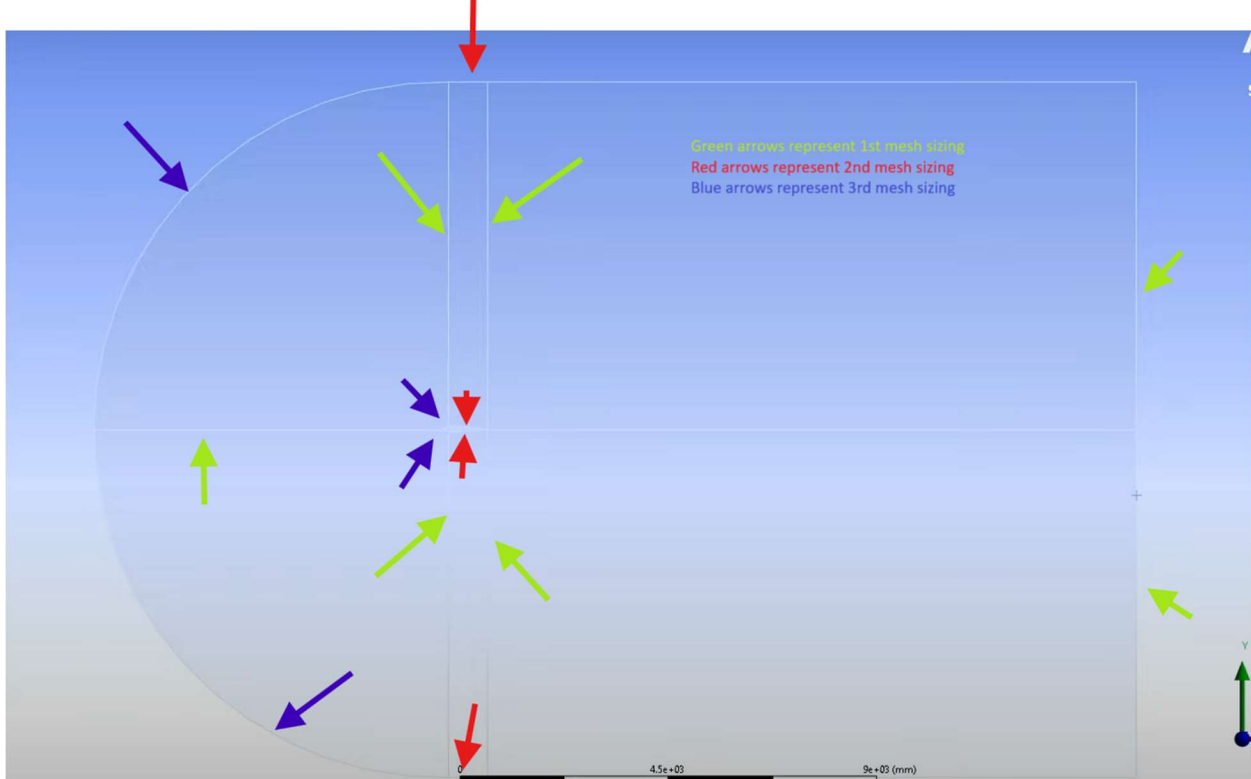


fig 10

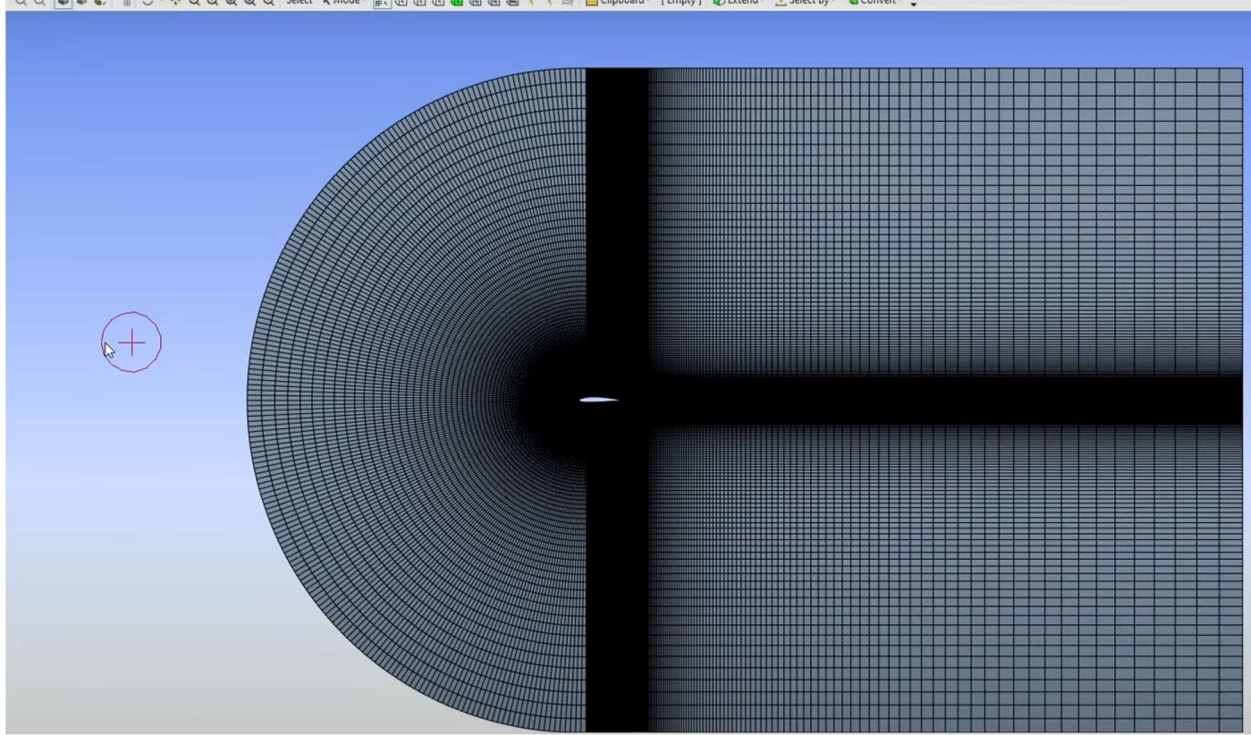
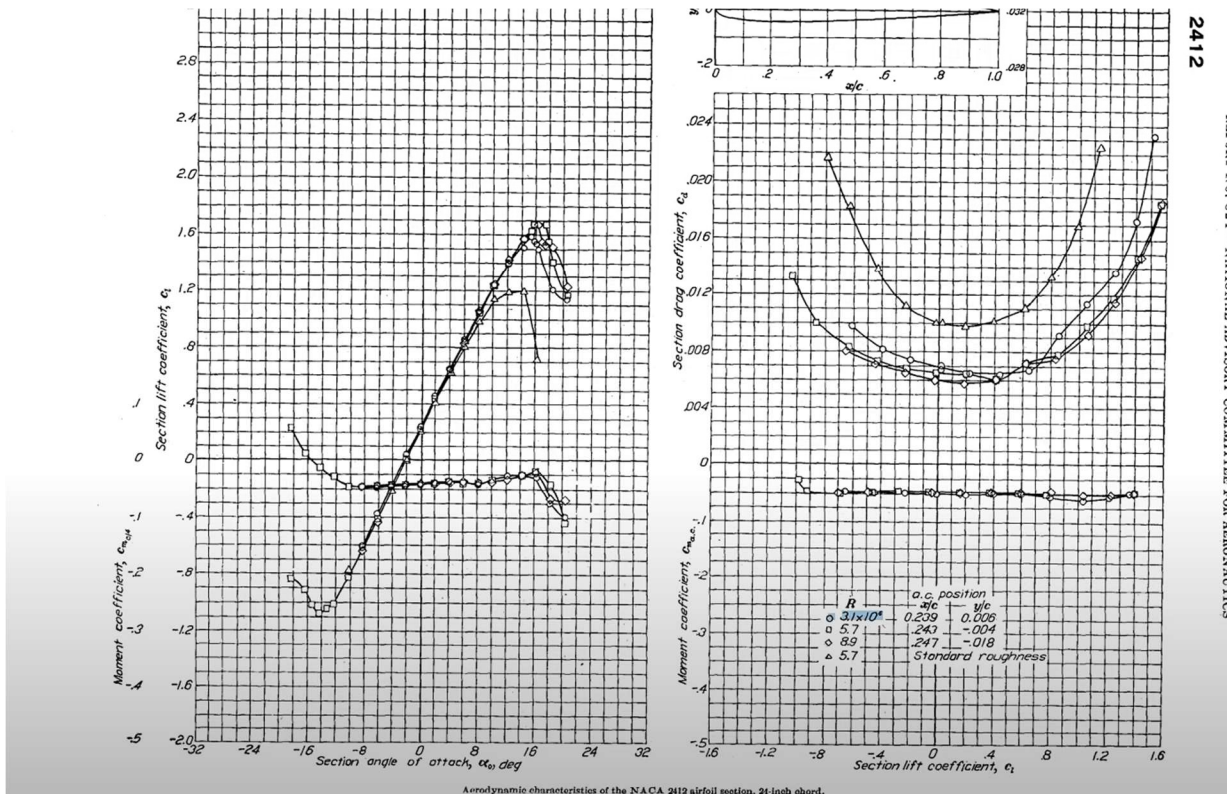


Fig 11



2412

STANDARDS FOR AVIATION AND SPACE AERONAUTICS

Fig 12

NACA2412

$$Re = \frac{\rho u L}{\mu}$$

$$\rho = 1.225 \text{ kg/m}^3 \quad L = 1 \text{ m} \quad \mu = 1.7225E-5$$

$$u = Re \times \mu / (L \times \rho)$$

at 15°C (288K) for air

$$u = 3.1E6 \times (1.802E-5) / (1 \times 1.225) = 45.6 \text{ m/s}$$

Fig 13

Correct Mesh Resolution	Input	Output
<p>It's important that your mesh near the wall is properly sized to ensure accurate simulation of the flowfield. This calculator computes the height of the first mesh cell off the wall required to achieve a desired Y^+ using flat-plate boundary layer theory.</p>	<p>Reset</p> <p>Compute</p> <p>$U_\infty:$ <input type="text" value="45.6"/> freestream velocity (m/s)</p> <p>$\rho:$ <input type="text" value="1.225"/> freestream density (kg/m³)</p> <p>$\mu:$ <input type="text" value="0.00001802"/> dynamic viscosity (kg/m s)</p> <p>$L:$ <input type="text" value="1.0"/> reference length (m)</p> <p>$y^+:$ <input type="text" value="1.0"/></p>	<p>Compute Wall Spacing</p> <p>$\Delta s:$ <input type="text" value="0.000008229051132519536"/> wall spacing (m)</p> <p>$Re:$ <input type="text" value="3099889.0122086573"/> Reynolds number</p> <p>Note: -1 indicates an input error</p>

Fig 14

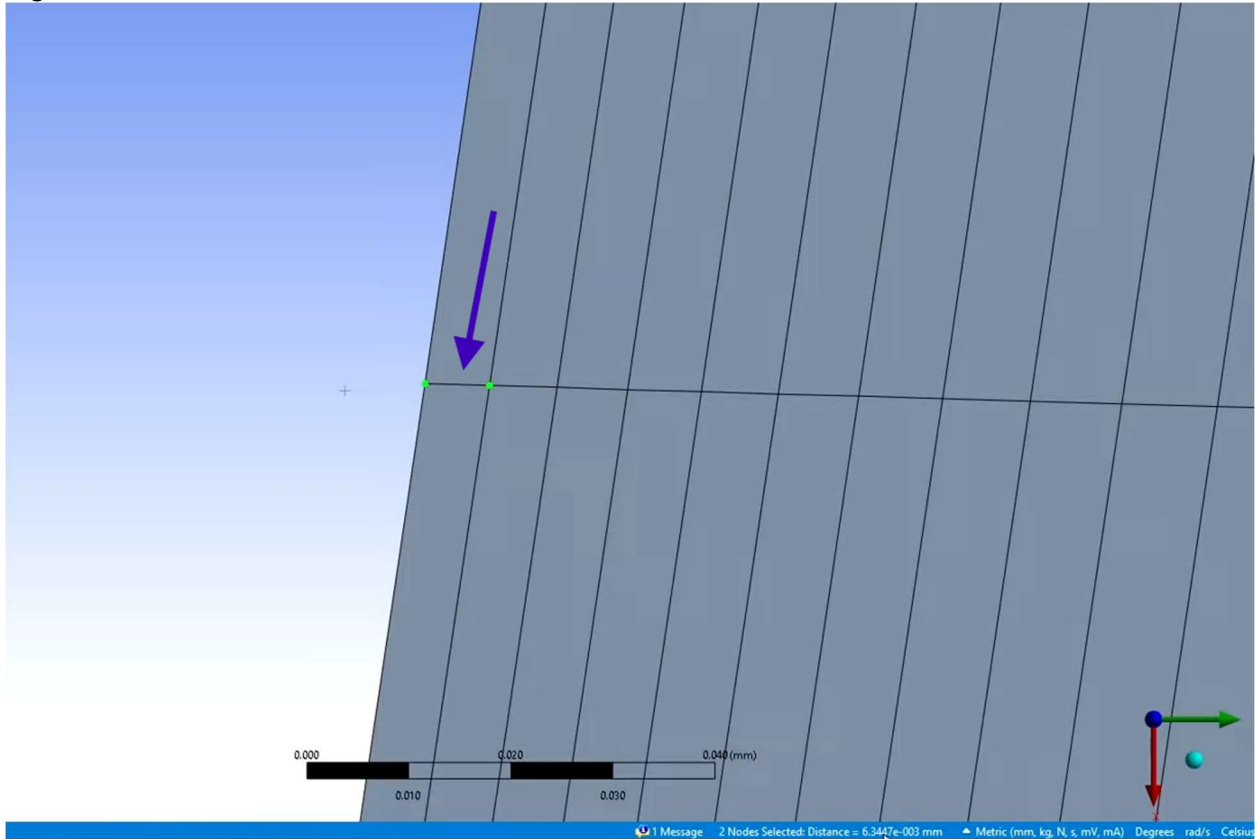


Fig 15

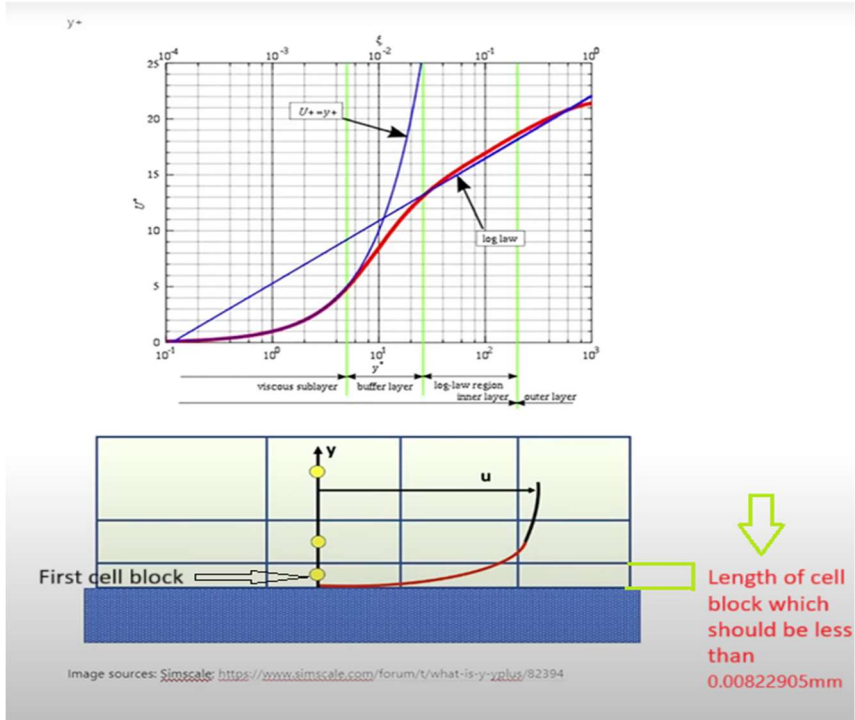


Fig 16

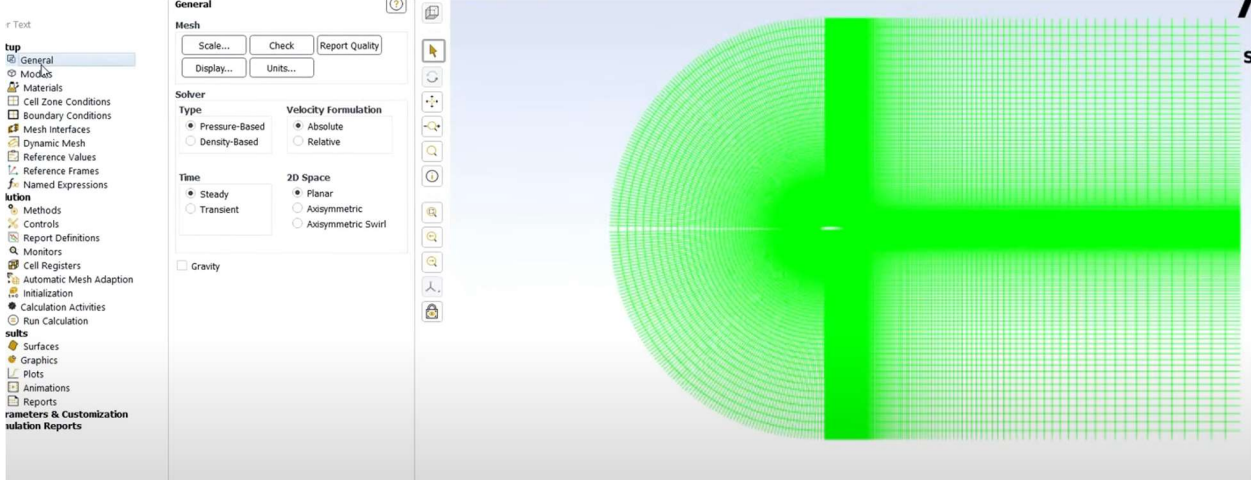


Fig 17

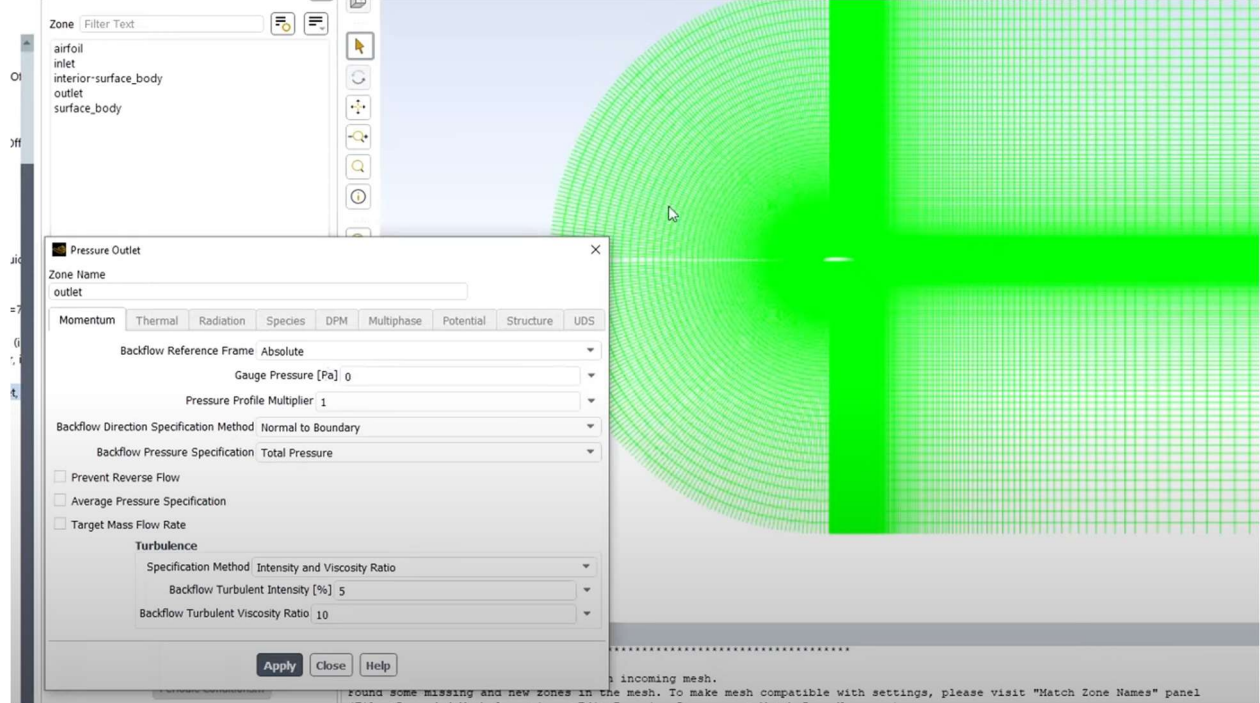


Fig 18

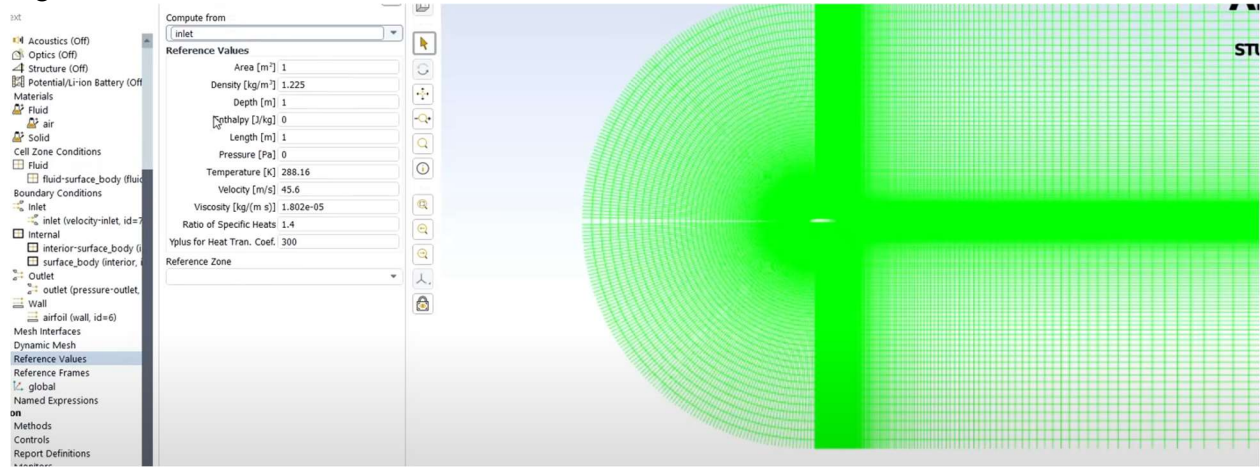


Fig 19

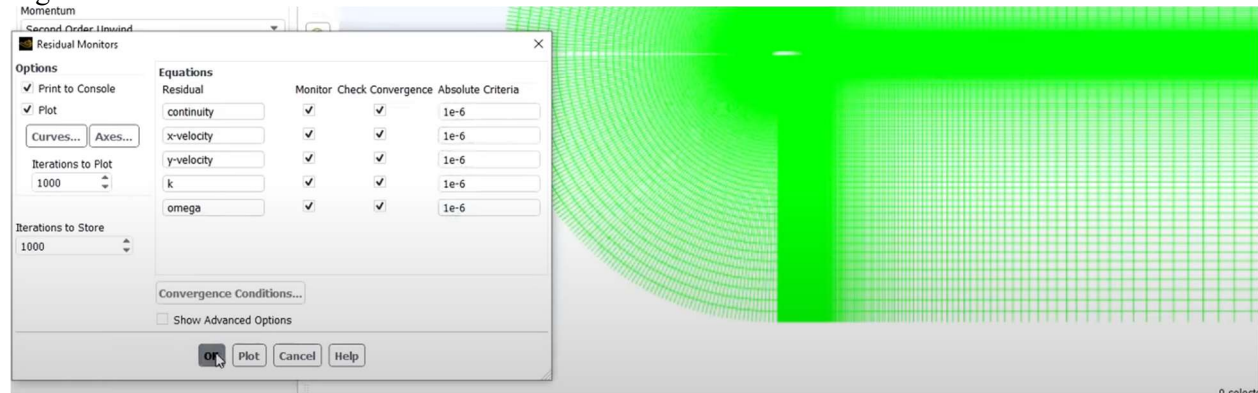


Fig 20

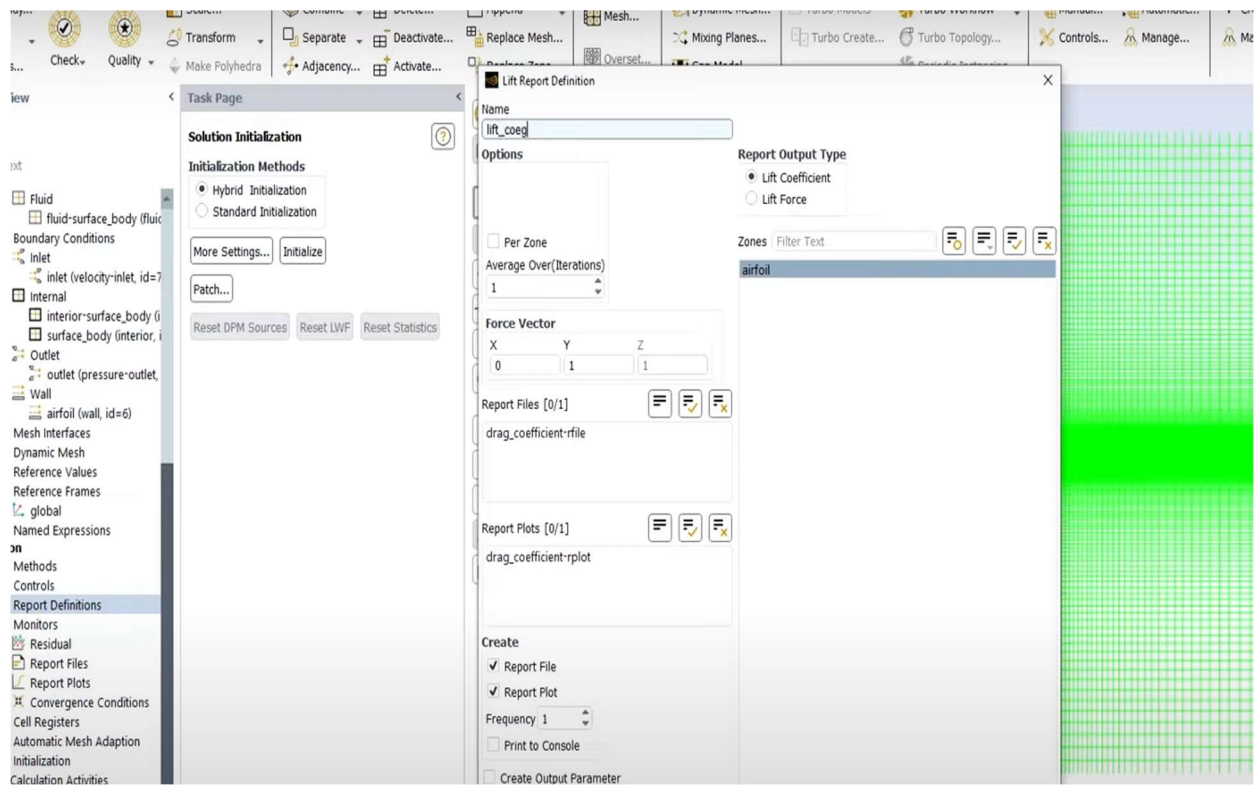


Fig 21

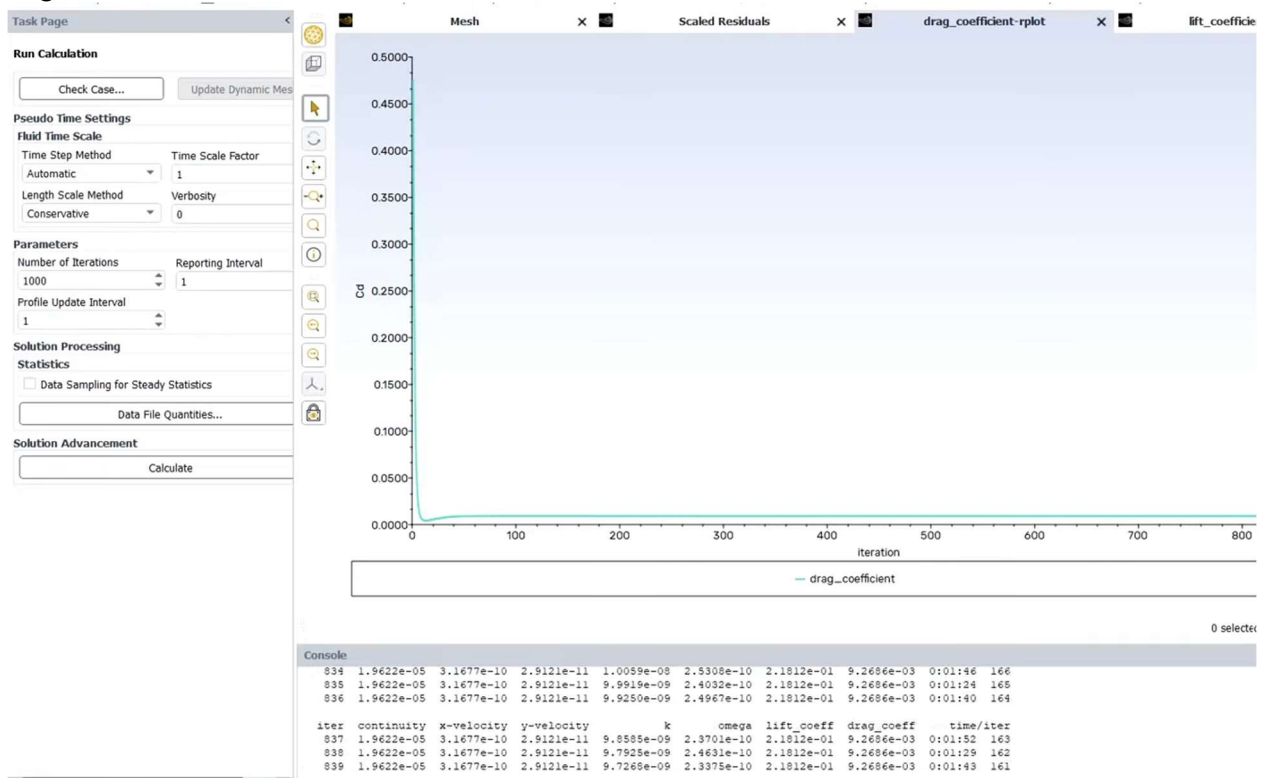
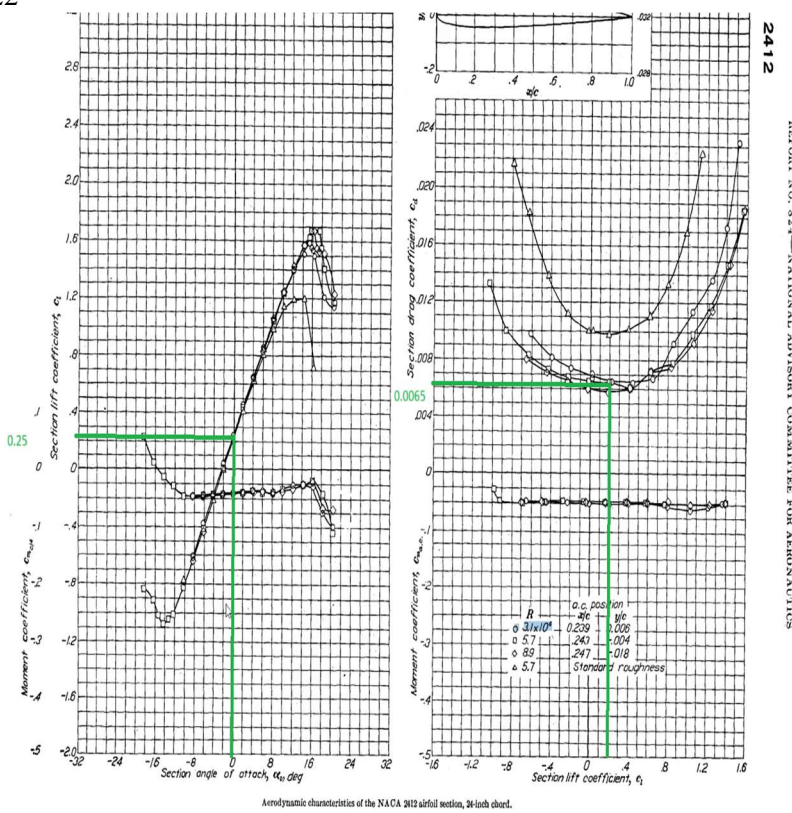


Fig 22



2412

NATIONAL ADVISORY COMMITTEE FOR AERONAUTICS

Fig 23

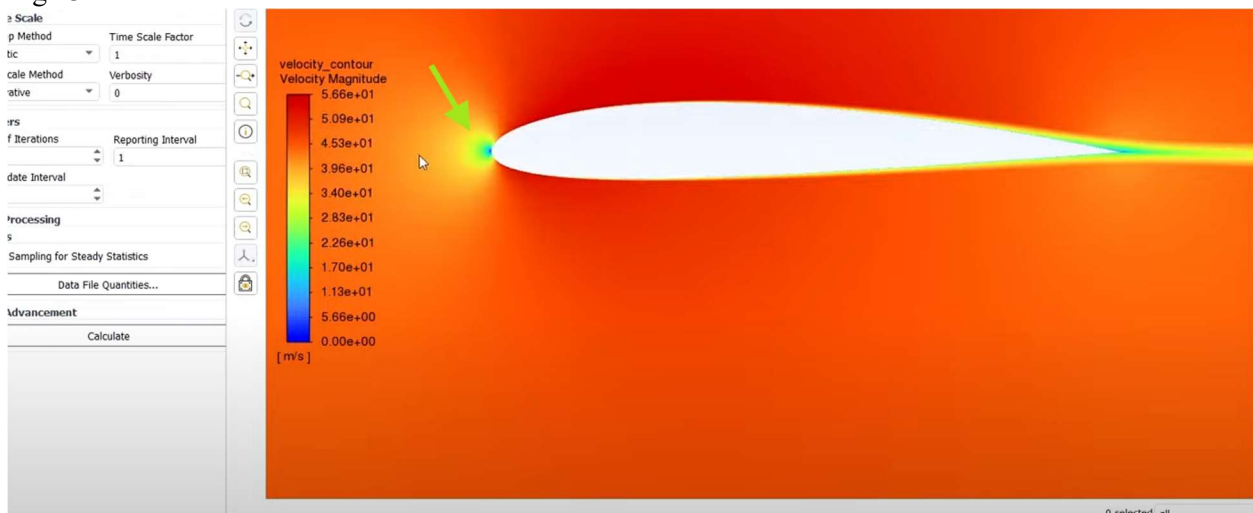


Fig 24

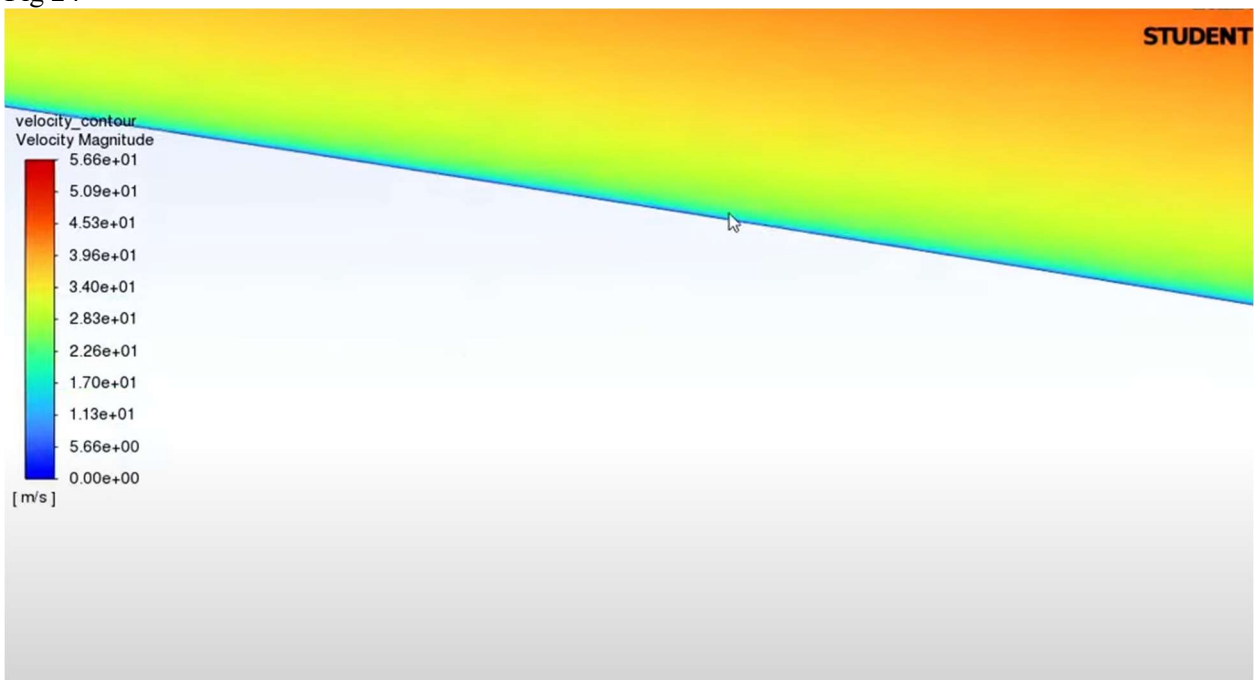


Fig 25

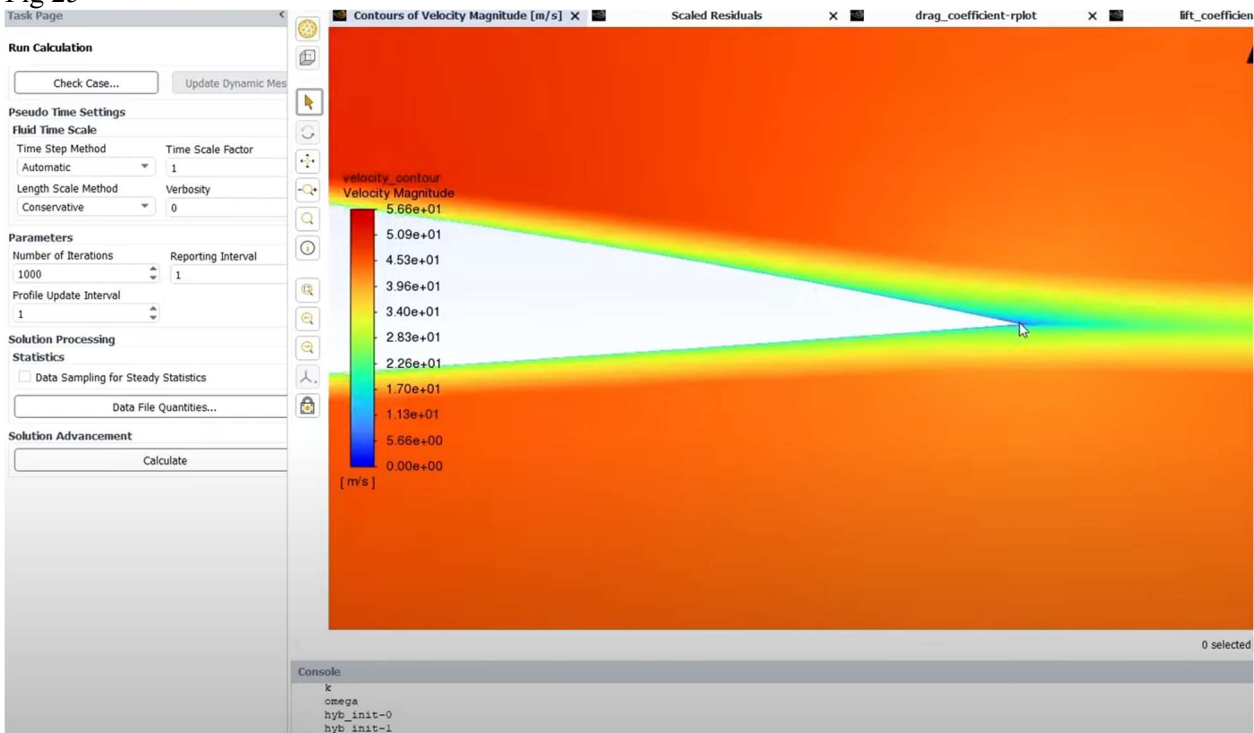


Fig 26

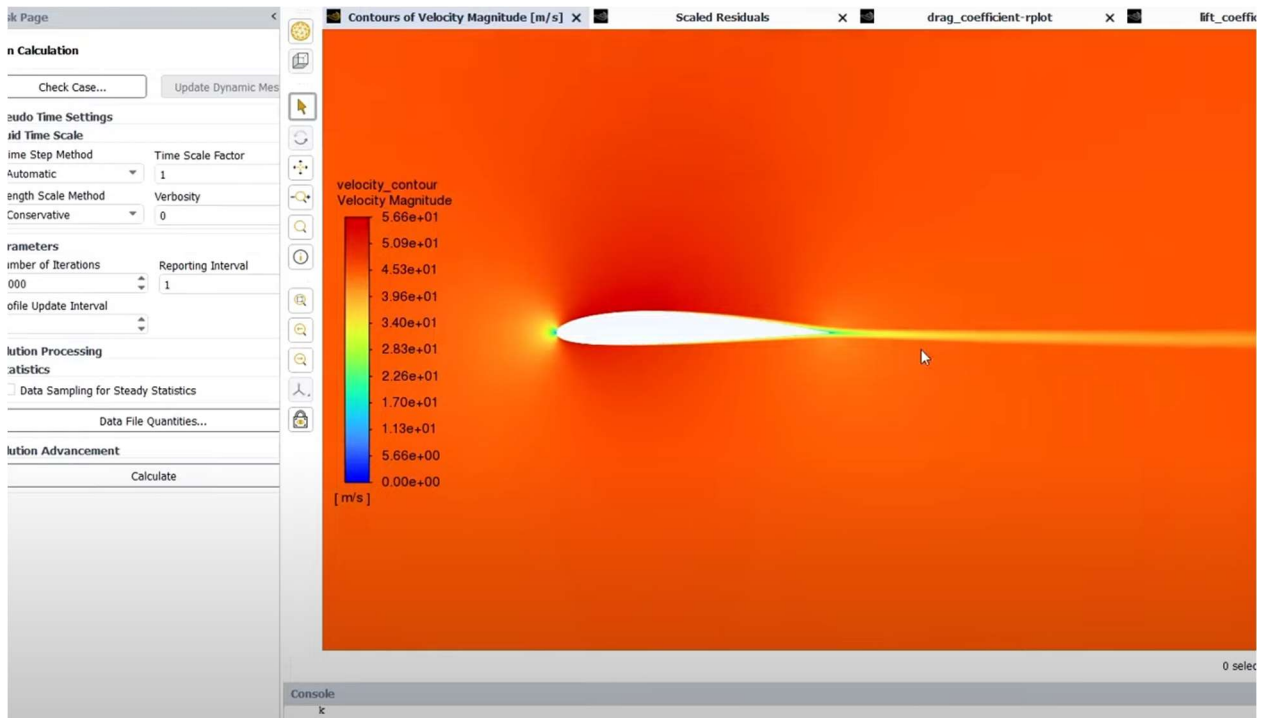


Fig 27

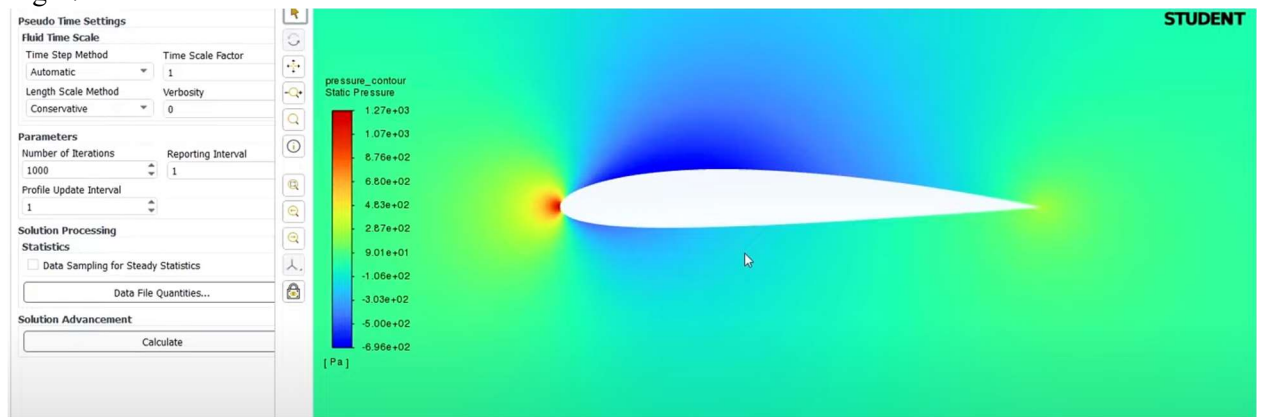


Fig 28

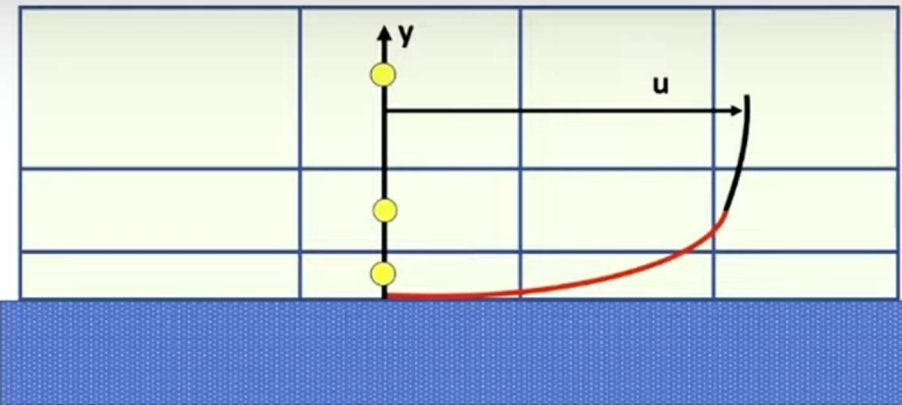


Image sources: Simscale; <https://www.simscale.com/forum/t/what-is-y-yplus/82394>

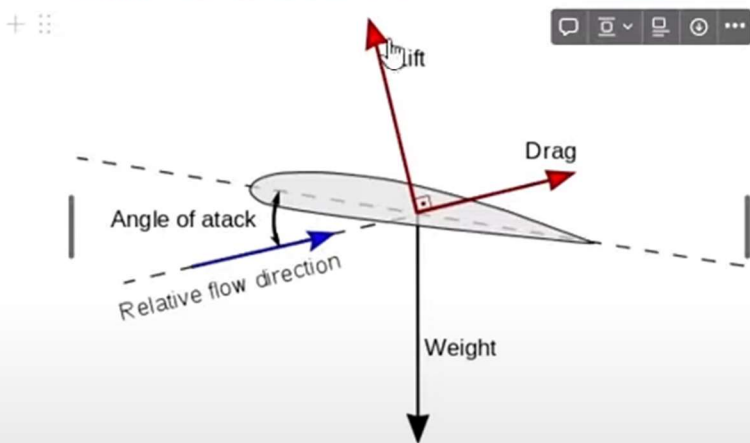


Image source:

https://en.wikiversity.org/wiki/Fluid_Mechanics_for_Mechanical_Engineers/Technical_Applications

Press 'space' for AI, '/' for commands...

Fig 29

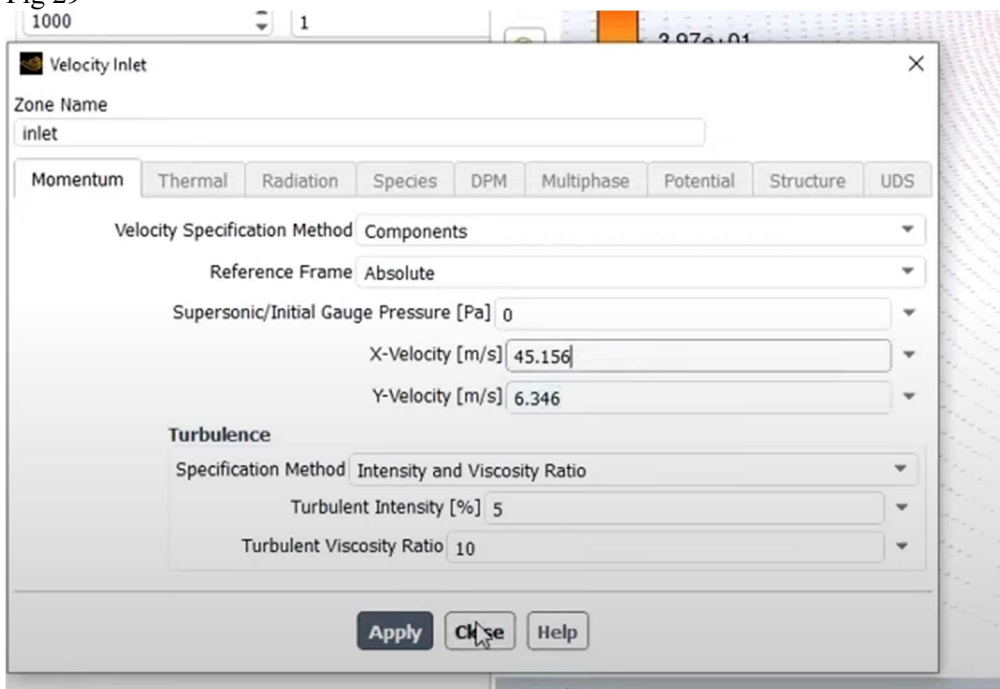


Fig 30

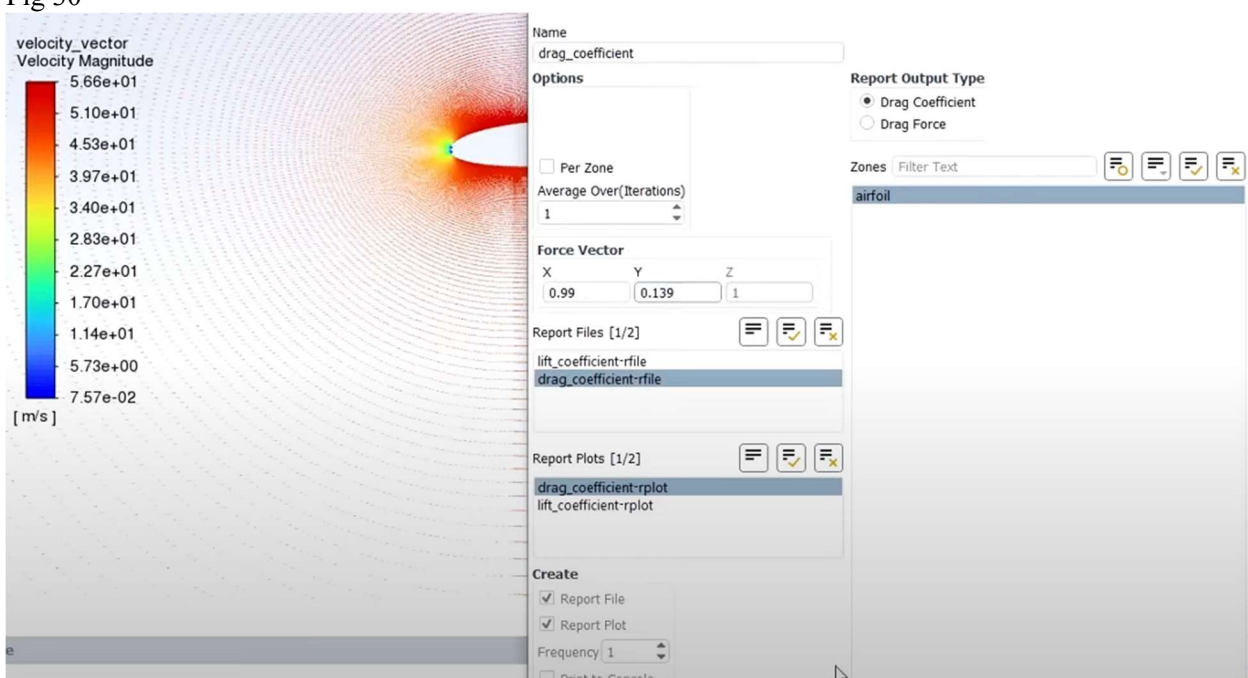


Fig 31

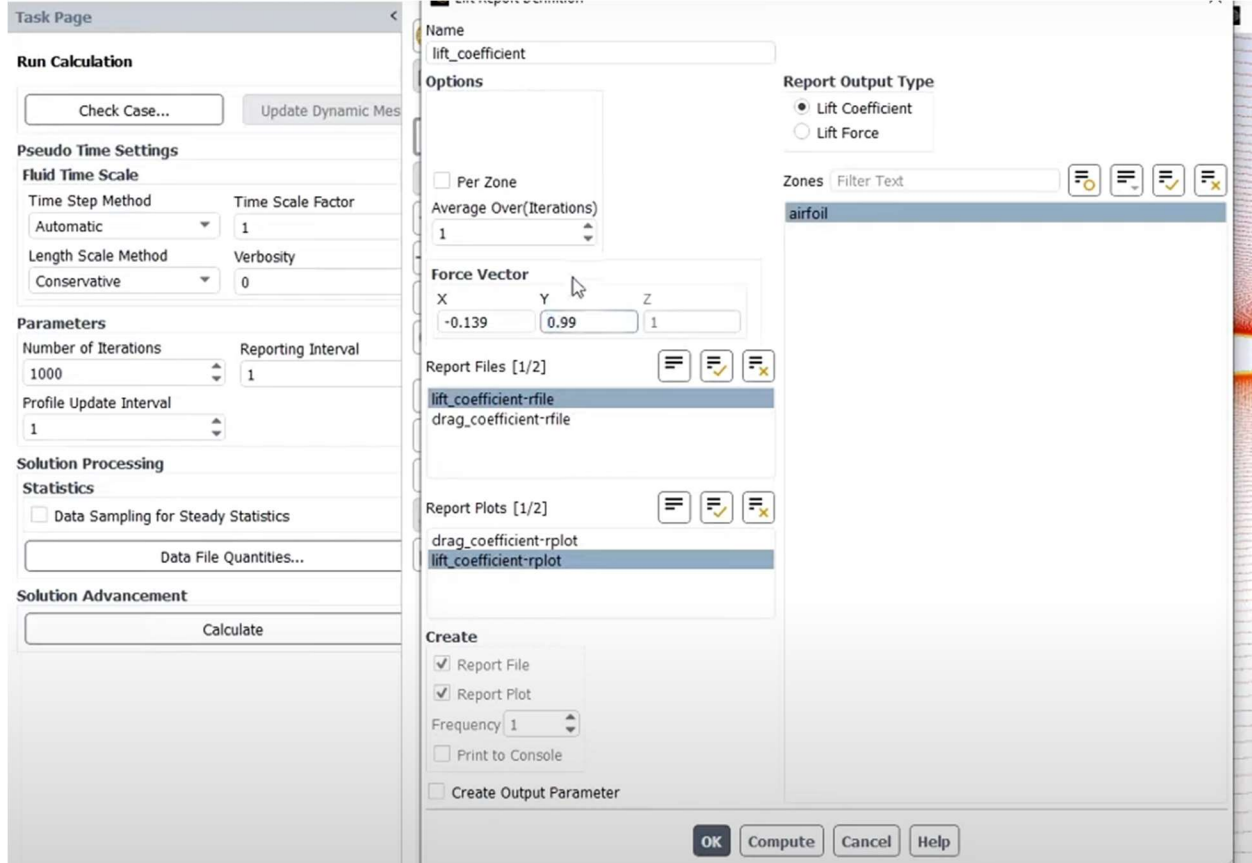


Fig 32

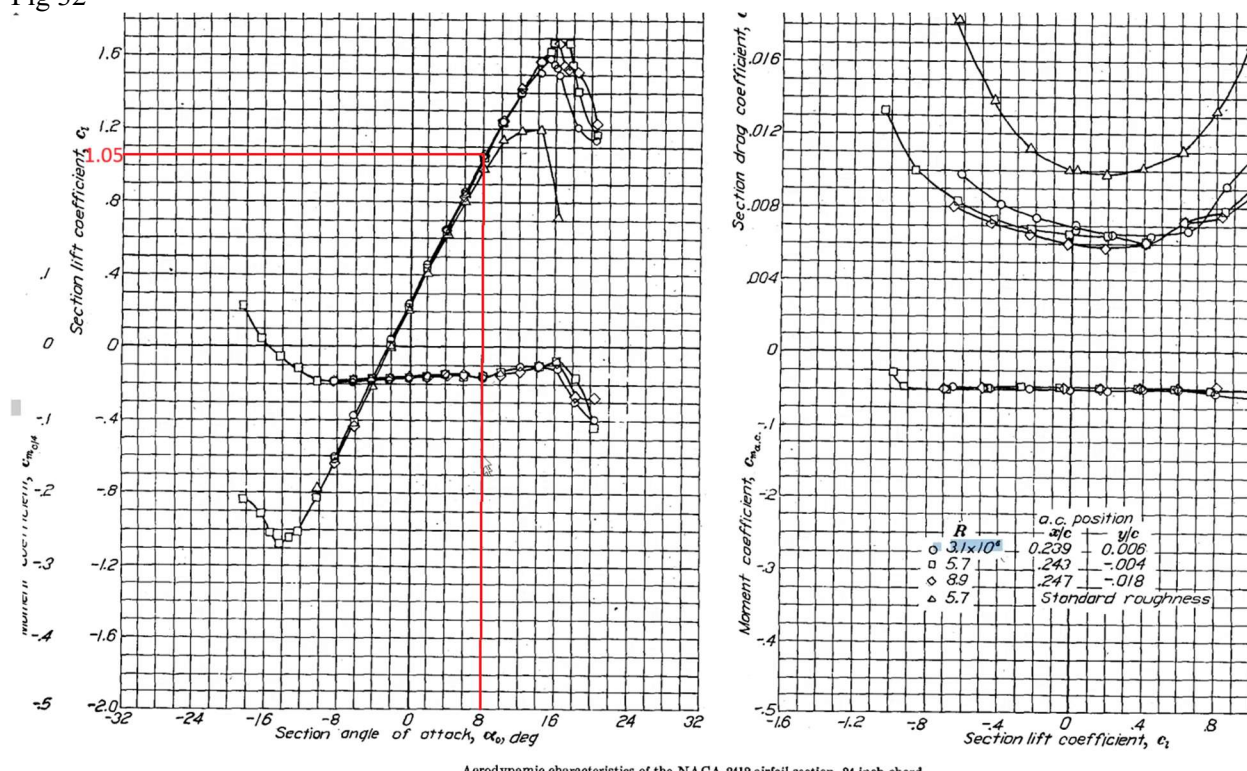


Fig 33

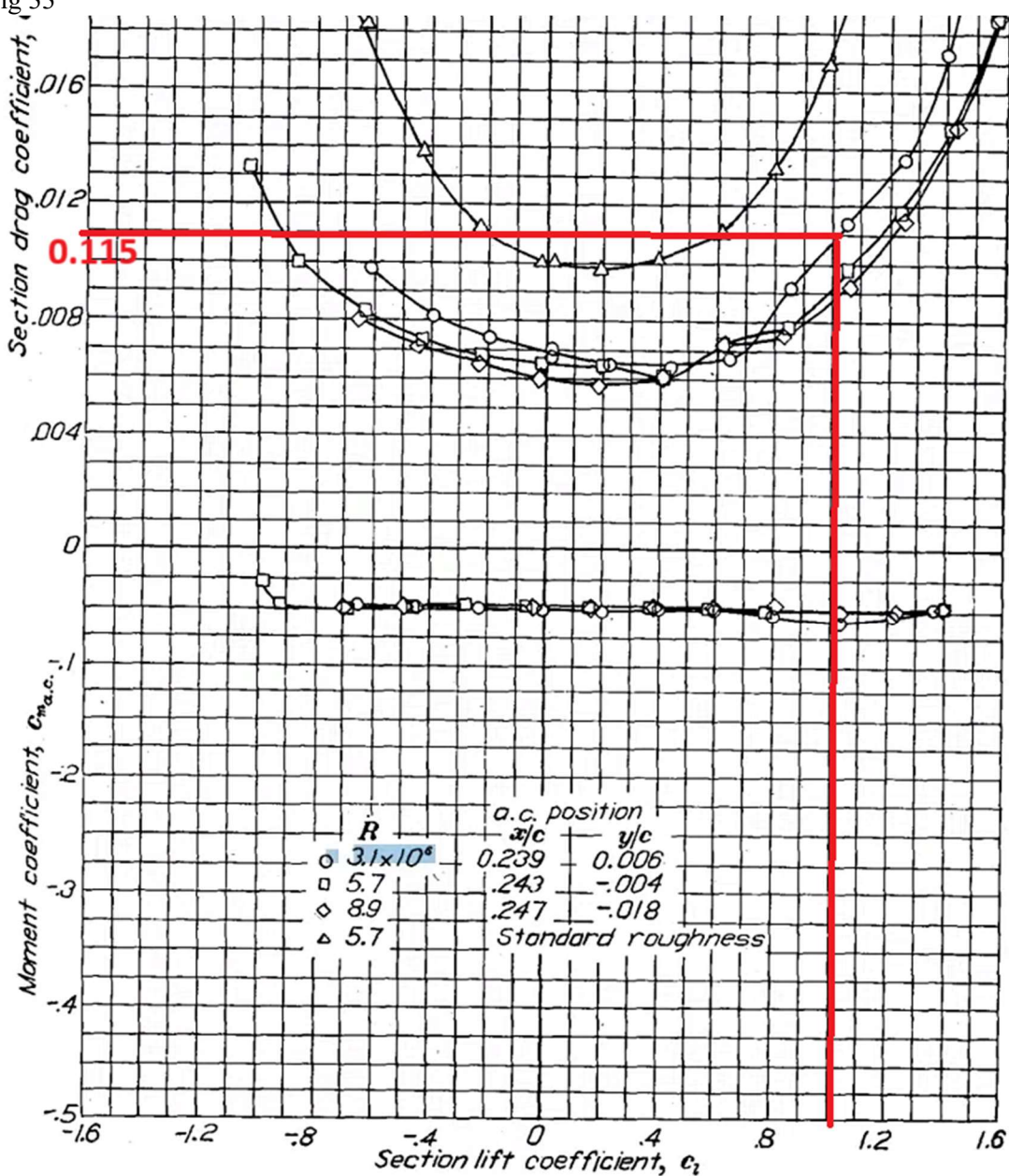


Fig 34

Console
iter continuity x-velocity y-velocity k omega lift_coeff drag_coeff time/iter
89 7.3432e-05 5.6719e-09 1.9533e-09 7.2539e-06 1.4515e-05 1.0490e+00 1.4165e-02 0:13:02 911
90 6.7019e-05 5.2414e-09 1.8510e-09 7.0506e-06 1.3557e-05 1.0490e+00 1.4165e-02 0:10:25 910
91 6.1200e-05 4.8711e-09 1.7598e-09 6.8705e-06 1.3482e-05 1.0490e+00 1.4166e-02 0:11:21 909
92 5.5851e-05 4.5467e-09 1.6883e-09 6.7088e-06 1.2998e-05 1.0490e+00 1.4166e-02 0:12:06 908
93 5.0809e-05 4.2190e-09 1.6208e-09 6.5641e-06 1.2554e-05 1.0490e+00 1.4166e-02 0:09:40 907
94 4.5610e-05 3.8797e-09 1.5618e-09 6.4358e-06 1.2127e-05 1.0491e+00 1.4167e-02 0:10:45 906
95 4.0940e-05 3.5303e-09 1.5071e-09 6.3215e-06 1.1720e-05 1.0491e+00 1.4167e-02 0:11:36 905

Fig 35

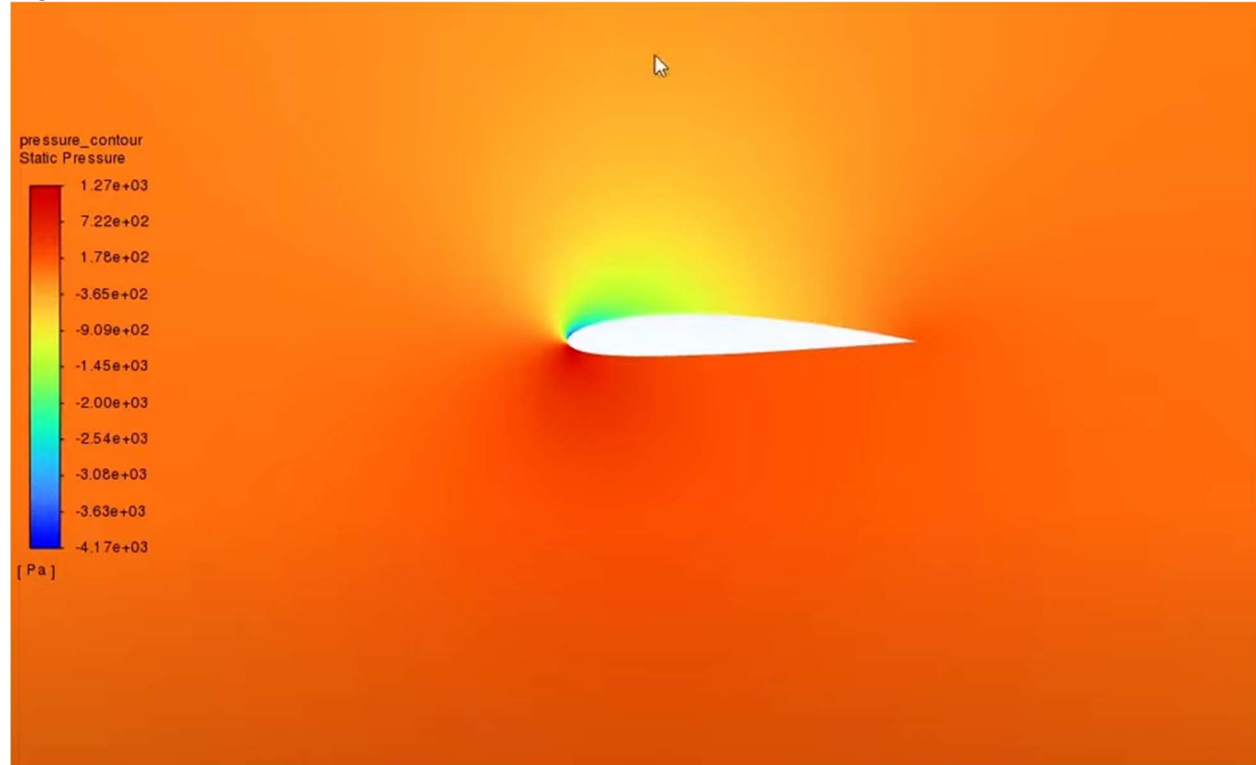


Fig 36

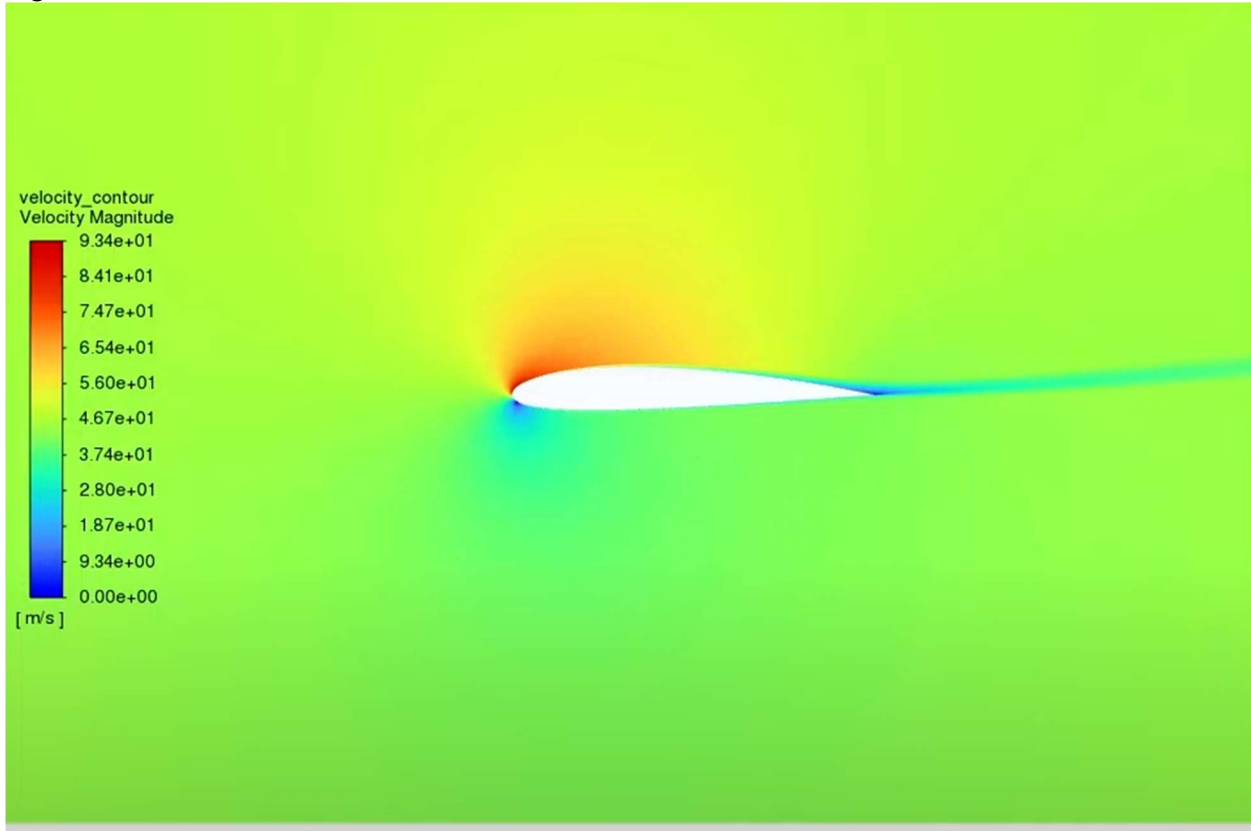


Fig 37

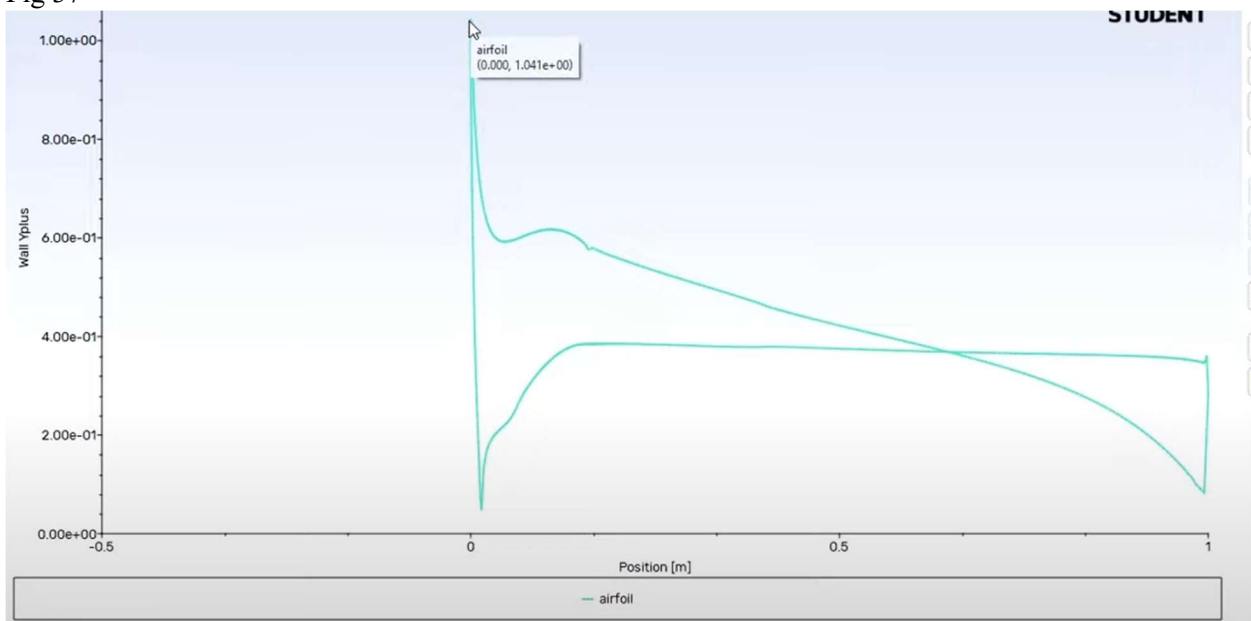


Fig 38

A	B	C	D	E	F	G	H	I	J
Angle of Attack (°)	Bias (Lift)	Random Error (Lift)	Measurement Uncertainty (Lift)	Total Uncertainty (Lift)	Bias (Drag)	Random Error (Drag)	Measurement Uncertainty (Drag)	Total Uncertainty (Drag)	
0	0.04	0.002	0.005	0.040360872	0.0027	0.0003	0.0005	0.002762245	
8	0.0009	0.0015	0.005	0.005297169	0.002667	0.0002	0.0005	0.002720825	

References

- National Aeronautics and Space Administration. (1993). Theory of Wing Sections (NACA Report No. 824). NASA Technical Reports Server. <https://ntrs.nasa.gov/citations/19930090976>
Abbott, I. H., & Von Doenhoff, A. E. (1959). *Theory of wing sections: Including a summary of airfoil data*. Dover Publications.
 - Anderson, J. D. (2010). *Fundamentals of aerodynamics* (5th ed.). McGraw-Hill Education.
 - Bertin, J. J., & Cummings, R. M. (2021). *Aerodynamics for engineers* (7th ed.). Pearson.
 - Clancy, L. J. (1975). *Aerodynamics*. Pitman Publishing.
 - Kuethe, A. M., & Chow, C.-Y. (1998). *Foundations of aerodynamics: Bases of aerodynamic design* (5th ed.). Wiley.
 - US Department of Energy. (2017). *Verification and validation of CFD simulations for nuclear reactor safety applications*. Office of Scientific and Technical Information (OSTI).
<https://www.osti.gov/servlets/purl/1368927>